Energy 219 (2021) 119686

Contents lists available at ScienceDirect

Energy

journal homepage: www.elsevier.com/locate/energy

# Molecular simulation of $N_2$ and $CO_2$ injection into a coal model containing adsorbed methane at different temperatures

Yang Bai, Hai-Fei Lin*, Shu-Gang Li**, Min Yan, Hang Long

*School of Safety Science and Engineering, Xi'an University of Science and Technology, 58, Yanta Mid. Rd., Xi'an, 710054, Shaanxi, PR China*

ARTICLE INFO

*Article history:*
Received 26 August 2020
Received in revised form
30 November 2020
Accepted 18 December 2020
Available online 22 December 2020

*Keywords:*
Gas injection displacement
Coalbed methane
Grand canonical Monte Carlo simulation
Mean square displacement
Diffusion coefficient
Diffusion activation energy

ABSTRACT

To research the dynamic mechanism of nitrogen and carbon dioxide displacement of methane, we used the grand canonical Monte Carlo (GCMC) simulation method to determine the lowest energy coal model containing adsorbed methane. The desorption behavior of $CH_4$ after the injection of $N_2$ and $CO_2$ at different temperatures was studied. Results show that $CO_2$ and $N_2$ were mainly used to drive off methane gas by occupying adsorption sites. The total energy of the $CH_4$-$CO_2$ model was lower than that of the $CH_4$-$N_2$ model. With the increased of temperature, the average relative concentration and motion velocity of $CH_4$ in the vacuum layer increased. The relationship of the average relative concentration and average velocity distribution of the three gases in the vacuum layer was $CH_4$>$CO_2$>$N_2$. Under the same time conditions, the relationship between the mean square displacement and diffusion coefficient of $CH_4$, $CO_2$, and $N_2$ in different models was $CH_4$>$CO_2$>$N_2$, and they all increased with temperature. The diffusion activation energy of $CH_4$ in the model injected with $CO_2$ was reduced by 20.53%, and the effect of injecting $CO_2$ to promote the desorption of methane was better than that of $N_2$.



## 1. Introduction

As an important fundamental issue, global energy resources have been included in the agenda of human production and life. Therefore, we should focus on how to make the best use of nonrenewable resources, including gas and oil coal. CBM(Coalbed methane) is composed mostly of methane ($CH_4$), with low amounts of $CO_2$, $N_2$, $O_2$, water vapor, and other gases. Therefore, of the existing clean energy, its utilization is considered to be an energy-saving and cost-effective alternative energy source. Currently, the co-mining research on CBM and coal is an important project worldwide [1]. On the other hand, the explosion of CBM directly threatens mining safety and productivity. To date, several difficult engineering problems limit the safe mining, separation, and utilization of CBM [2].

Coal is a complex material composed of inorganic matter and organic matter, which has complex internal surface structure characteristics. Determining the interaction mechanism between coal and gas from the molecular level has always been a fundamental problem in the research and development of CBM [3,4]. Coalbed methane mainly exists in coal seam in the adsorbed state and partially exists in the cracks and pores of the coal seam in the free state. After the displacement gases are injected into the coal seam, they can drive and replace the coalbed methane, promote the desorption and seepage of the CBM, and facilitate the efficient extraction of CBM. In the process of gas injection displacement, coal seam temperature, pore size, type of injected gases, pressure, and other factors can affect the structural evolution of coal seam pores and fissures and the desorption of CBM.

To reveal the mechanism of desorption kinetics of gas-displacing coalbed methane, experts and scholars at home and abroad have gradually started to research the kinetics of adsorption and desorption in recent years [5]. Kumar et al. [6] compared and analyzed the application status of gas injection displacement coalbed methane technology from three aspects (gas injection position, gas injection mode, and gas injection type). Wang Q and Bhowmik [7,8] studied the effect of high-pressure carbon dioxide fluid on coalbed methane recovery. K Jessen and Han F [9,10]conducted a comparative experiment of competitive adsorption and displacement adsorption of $CO_2$, $N_2$, and gas mixture injected into the coal seam and verified it with a numerical simulation method. Fan Y and Zhang DF [11,12] investigated the adsorption performance of $CH_4$, $N_2$, and $CO_2$ and the displacement behavior of shale

* Corresponding author.
** Corresponding author.
*E-mail addresses:* lhaifei@xust.edu.cn (H.-F. Lin), lisg@xust.edu.cn (S.-G. Li).

https://doi.org/10.1016/j.energy.2020.119686
0360-5442/

adsorption of $CH_4$ by $CO_2$ injection. Kong L et al. [13] conducted a simulation experiment of carbon dioxide/nitrogen injection to promote the emission of coalbed methane under uniaxial stress and layered pre-compression molding conditions and then derived a coupled mathematical model of carbon dioxide/nitrogen displacement of coalbed methane. Topolnicki et al. [14] established a numerical model describing the kinetics of the $CO_2/CH_4$ exchange adsorption process on briquette and compared it with the experimental results. Mohammad et al. [15] used a dual pore/permeability model and the local grid refinement (LGR) method to perform numerical simulation of $CO_2$ displacement of coalbed methane. Crosdale P, Wang Z, Charoensuppanimit P, and Guan C [16-19] employed experimental methods and theoretical analysis to research the effect of temperature on methane adsorption capacity.

As a theoretical research method, molecular simulation has been paid close attention in the study of adsorption properties [20]. The microscopic adsorption mechanism between the adsorbent and adsorbate can be studied at the molecular level by computer molecular simulation [21]. Matranga and Liu X et al. [22,23] used the Monte Carlo method to simulate the adsorption behavior of $CH_4$, $CO_2$, and $N_2$ on activated carbon. Their results showed that the adsorption capacity and adsorption heat of $CO_2$ are higher than those of $CH_4$, $N_2$. Mosher et al. [24] used molecular simulation to study the competitive adsorption of $CH_4$ and $CO_2$ in the micropore and mesoporous structure of coal. Hu et al. and You et al. [25,26] studied the self-diffusion and inter-diffusion of $CO_2$ and $CH_4$ multicomponent gases by molecular simulation. Sun X et al. [27] established a new MS-BPD pore diffusion model to research the adsorption and diffusion of multi-component gas during gas injection and analyzed the effect of multi-component gas injection on coalbed methane recovery. Liu Y and Yang J [28,29] used molecular simulation techniques to research the effect of temperature on methane adsorption capacity and gas adsorption density in pores of different sizes. Tao H and Liu X [30,31] researched the competitive adsorption and selective diffusion of $CH_4$, $CO_2$, and $N_2$ in coal by molecular dynamics simulation.

At present, numerous studies have discussed coalbed methane desorption in the process of gas injection displacement. Most of them were carried out through laboratory and industrial experiments, which cannot completely reflect the gas injection displacement process. The molecular mechanism of desorption of coalbed methane by injected gas needs to be further clarified. The use of molecular simulation techniques to research the interaction mechanism of gases from a micro perspective also needs to be improved. Therefore, the effect of $N_2$ and $CO_2$ injection on the desorption kinetics of $CH_4$ in coal models containing adsorbed coalbed methane should be further analyzed to gain a deeper understanding of the mechanism of $CH_4$ desorption. In this paper, a model reflecting the actual coal structure was established, and molecular simulation was used to research the interaction between gases after $CO_2$ and $N_2$ injection into the coal model containing the adsorbed CBM from a microscopic perspective. The GCMC method was used to simulate the desorption behavior of $CH_4$ after the injection of $N_2$ and $CO_2$ in a coal model containing adsorbed CBM at different temperatures were studied for the first time. This work provides a theoretical basis for further clarifying the mechanism of $CH_4$ displacement by $N_2$ and $CO_2$ in coal seam.

## 2. Methodology

### 2.1. Models

In this study, simulations were conducted using Accelrys Materials Studio software (http://accelrys.com). Coal is a porous material that is composed of various cross-linked molecules with a high molecular weight. The coal model was based on the Wiser (USA) model ($C_{184}H_{155}N_3O_{20}S_3$) [32], and it was used to explore the interactions between coal and $CH_4$, $H_2O$, and $N_2$. This model considered the size of the aromatic nuclei in the coal, and the existing forms of elements are C, H, O, N, and S. This model can fully reflect the structural characteristics of the coal. The Wiser coal molecular model is recognized as a reasonable bituminous coal molecular model. The mass percentages of each element in the model were: C was 78.3 wt%, O was 11.2 wt%, H was 5.8 wt%, S was 3.2 wt%, and N was 1.4 wt%, which were close to the measured data [33].

In this paper, the COMPASS force field [34] was used to describe the interaction between molecules and atoms in the system. COMPASS ( Condensed-phase Optimized Molecular Potentials for Atomistic Simulation Studies ) force field was a condensed-phase optimized ab-initio force field [35]. Yin T [36] and Hu H [37] chose this field to simulate the interaction between coal structure and gas, and the field was applicable to all kinds of alkanes and gases such as nitrogen and carbon dioxide. The interaction formula is as follows [34].

$$E_{total} = E_{valence} + E_{non-bond} \quad (1)$$

In the formula, $E_{total}$ is the total energy of the composite material system, $E_{valence}$ is the bond interaction energy of the composite material system, bond energy (E) is the measure of bond strength in a chemical bond. And $E_{non\text{-}bond}$ is the non-bond interaction energy of the composite material system. The bond-to-bond interaction energy can be divided into various forms according to energy components, and the expression is as follows [34].

$$E_{valence} = E_b + E_\theta + E_\phi + E_\omega + E_c \quad (2)$$

In the formula, $E_b$ is the stretching vibration energy of the bond length, $E_\theta$ is the bending vibration energy of the bond angle, $E_\phi$ is the torsional vibration energy of the dihedral angle, $E_\omega$ is the out-of-plane angular offset vibration energy, and $E_c$ is the cross-coupling energy between bond interactions. The non-bond interaction energy ($E_{non\text{-}bond}$) includes Van der Waals energy ($E_v$), Coulomb interaction energy ($E_e$), and hydrogen bond interaction ($E_h$), and its expression is as follows [34].

$$E_{non-bond} = E_v + E_e + E_h \quad (3)$$

In physical chemistry, the van der Waals forces are distance dependent interactions between atoms [38]. Coulomb force, also called electrostatic force or Coulomb interaction, attraction or repulsion of particles or objects because of their electric charge [39]. A hydrogen bond is the electrostatic attraction between two polar groups that occurs when a hydrogen (H) atom covalently bound to a highly electronegative atom such as nitrogen (N), oxygen (O), or fluorine (F) experiences the electrostatic field of another highly electronegative atom nearby [40]. The calculation methods of force fields and energies are listed in the supporting information of this paper.

### 2.2. Model optimization and rationality verification

Before adsorption simulation, the crystal cells containing two coal molecules were first constructed, and the structure of the model was optimized. Moreover, the geometry optimization module of Forcite, the molecular dynamics module, was used to optimize the structure of the model. The initial configuration was an optimized coal model with the lowest energy and without adsorbate molecules. On the basis of the change in energy, the

Metropolis operation rules were applied to accept or reject the change for forming a new configuration. A periodic boundary condition was used in three dimensions, and the cell parameters were as follows: $a = b = c = 21.7706$ Å and $\alpha = \beta = \gamma = 90°$.

The parameters for geometry optimization were as follows. The optimization method was set to medium, the selected force field was COMPASS, the Ewald method was used to calculate the Coulomb force, and an atom-based method was used to calculate the van der Waals force and hydrogen bonding. After optimization of molecular mechanics, a model with local energy minimization was obtained. Therefore, annealing dynamics simulation is necessary to globally optimize the model on the entire potential energy surface to obtain a global energy minimization configuration. The cell was expanded to construct a $1 \times 2 \times 2$ supercell, and a 5 nm vacuum layer was added. When the energy of the system was the lowest, the calculated model density was 1.23 g/cm$^3$. This value was consistent with the actual density of bituminous coal in the literature (1.2-1.4 g/cm$^3$) [41], indicating that the optimized coal molecular spatial structure was reasonable. The constructed slit model is shown in Fig. 1. It shows the process of constructing the wiser model from a single molecule to a single cell model and expanding it to a super cell after optimization. Fig. 1a is the single molecule Wiser model, Fig. 1b is the optimized crystal cell containing two coal molecules, and Fig. 1c is the supercell model after the crystal cell is expanded.

### 2.3. Screening of coal model containing adsorbed methane

To determine the lowest energy of the coal model containing adsorbed methane, the adsorption characteristics of supercells were calculated. The setting parameters of the sorption module were as follows: The task item was adsorption isotherm, the simulated load balancing step was $1 \times 10^6$ steps, the total number of steps was $2 \times 10^6$, the calculation method was Metropolis, the QEq method was used to calculate the charge, the Ewald method was applied to compute the electrostatic interaction between atoms, and the atom-based method was used to calculate the van der Waals interaction and hydrogen bonding. Adsorption characteristic parameters from three simulation calculations are shown in Table 1.

By comparing the data in Table 1, the lowest energy model A was selected as the coal model containing adsorbed methane in this paper. The relationship between adsorption capacity and adsorption heat with pressure in each model is shown in Fig. 2. Fig. 2a is the relationship between adsorption capacity with the pressure of the coal model containing adsorbed methane under different temperatures. The adsorption configurations of methane in the model at different temperatures are also shown. Fig. 2b is the relationship between adsorption heat with pressure under different temperatures. It also shows the distribution of methane density in the model at different temperatures.

As shown in Fig. 2a, the average adsorption capacity increased with the increase in pressure and decreased with the increase in temperature. In Fig. 2b, the average adsorption heat decreased with increasing pressure. However, the reduction range was small at only 0.3 kcal/mol, and the average adsorption heat decreased as the temperature increased.

### 2.4. Simulation of adding different displacement gases into coal containing adsorbed methane

To determine the number of $CO_2$ and $N_2$ injected into the model constructed in Section 2.3, the adsorption simulation of $CO_2$ and $N_2$ under 1 MPa at 303 K was carried out. Given that the high temperature was not conducive to adsorption, the adsorption capacity at 303 K was the largest in the simulated temperature range. Therefore, the simulation temperature of $CO_2$ and $N_2$ was set to 303 K. Through simulation calculations, the adsorption results of $CO_2$ and $N_2$ injected into the model separately are shown in Table 2.

In the simulations for promoting methane desorption in coal models under different temperature conditions, the numbers of injected $CO_2$ and $N_2$ were 225 and 63 n/per cell, respectively. The initial configuration of the simulation is to add different numbers of $CO_2$ and $N_2$ on the basis of the model in Section 2.3 and then perform the next simulation. The Focite module was used for the dynamic calculation of the model, and the NVT system was adopted in the optimization process.

The setting parameters of the Focite module were as follows. The task item was dynamics, the temperature was set at 303-343 K, the temperature control method was Nose, the pressure control method was Berendsen, the number of steps was 10,000, the time step length was 1 fs, and the simulation time was 40 ps.

## 3. Results and discussion

### 3.1. Comparative analysis of total energy and relative concentration of desorption configuration of coal model at different temperatures

The desorption simulation under different temperature and pressure was carried out by the models injected with $CO_2$ and $N_2$. The total energy of the initial model and the desorption model after gas injection was obtained, as shown in Fig. 3.

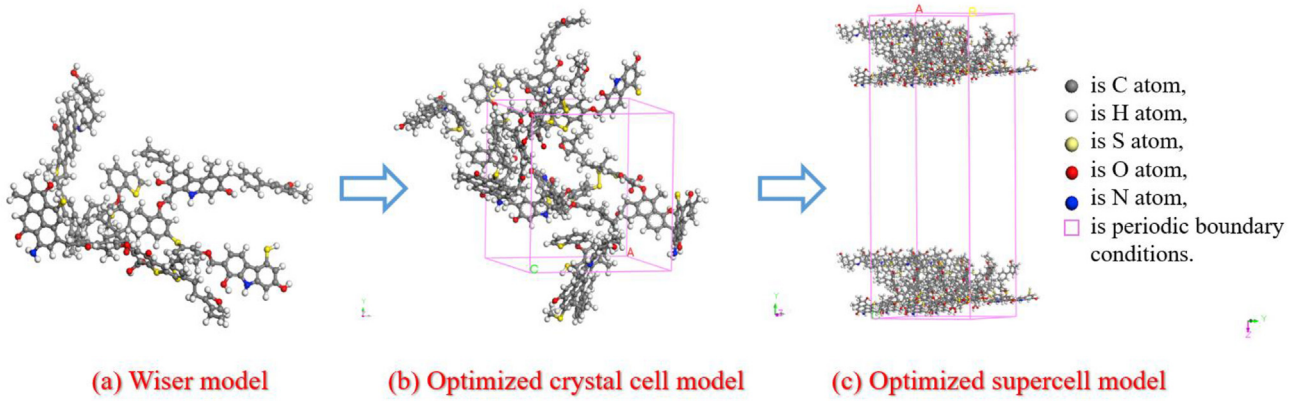


**Fig. 1.** The constructed slit model.

**Table 1**
Adsorption characteristic parameters from three simulation calculations of coal model containing adsorbed methane.

| Temperatures(K) | No. | Total energy (kcal/mol) | Average adsorption capacity (n/per cell) | Isosteric heats of adsorption (kcal/mol) |
|---|---|---|---|---|
| 303 | A | −260.666 | 104.583 | 3.386 |
| | B | −253.334 | 103.641 | 3.336 |
| | C | −259.053 | 104.727 | 3.367 |
| 313 | A | −230.075 | 94.185 | 3.339 |
| | B | −228.340 | 94.385 | 3.319 |
| | C | −221.695 | 92.511 | 3.295 |
| 323 | A | −196.055 | 83.579 | 3.253 |
| | B | −190.178 | 82.298 | 3.216 |
| | C | −188.695 | 81.203 | 3.227 |
| 333 | A | −176.502 | 76.340 | 3.230 |
| | B | −172.922 | 75.010 | 3.219 |
| | C | −170.059 | 74.426 | 3.199 |
| 343 | A | −151.944 | 68.214 | 3.153 |
| | B | −147.587 | 67.009 | 3.126 |
| | C | −151.555 | 67.944 | 3.155 |

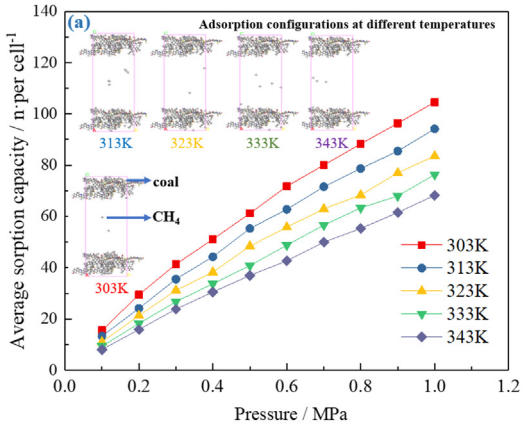


(a) The relationship between adsorption capacity with pressure.

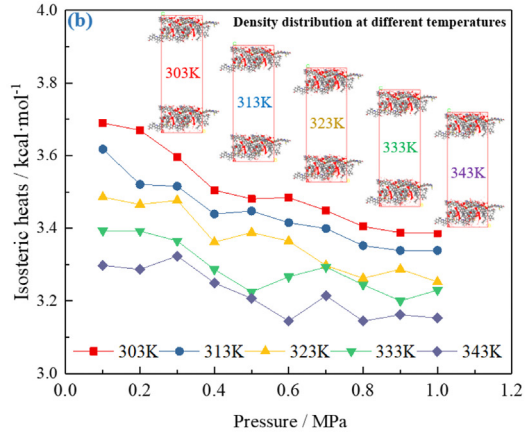


(b) The relationship between adsorption heat with pressure.

**Fig. 2.** The relationship between adsorption capacity and adsorption heat with pressure in each model.

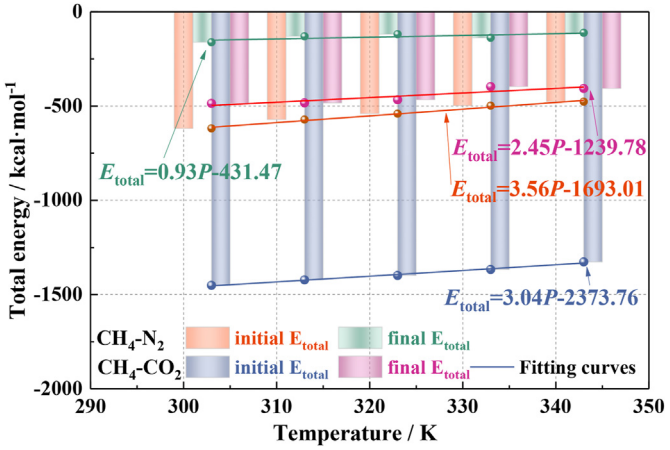


**Fig. 3.** The total energy of the initial model and the desorption model after gas injection.

As shown in Fig. 3, the total energy of the initial model and desorption model of the $CH_4$-$N_2$ and $CH_4$-$CO_2$ systems both increased with the increase of temperature, and presented a linear positive correlation with the temperature. After desorption of $CH_4$-$N_2$ and $CH_4$-$CO_2$ configurations, the total energy of the system increased, indicating that desorption was an endothermic reaction. At the temperature of 303-343K, compared with the initial configuration, the total energy growth rates of the desorption configuration of $CH_4$-$N_2$ were 73.87%(303K), 77.33%(313K), 78.05%(323K), 72.43%(333K), and 76.65%(343K). The total energy growth rates of the desorption configurations of $CH_4$-$CO_2$ were 66.51%(303K), 66.01%(313K), 66.64%(323K), 70.97%(333K), and 69.35%(343K). The total energy of the $CH_4$-$CO_2$ model was lower than that of the $CH_4$-$N_2$ model, which showed that the $CH_4$-$CO_2$ model was more stable than the $CH_4$-$N_2$ model from a microscopic perspective.

To further study the distribution of $CH_4$, $CO_2$, and $N_2$ in the coal

**Table 2**
Adsorption characteristic parameters of $CO_2$ and $N_2$ injected into the model.

| Type of gases | Total energy (kcal/mol) | Average adsorption capacity (n/per cell) | Isosteric heats of adsorption (kcal/mol) |
|---|---|---|---|
| $CH_4$-$N_2$ | −117.223 | 63 ($N_2$) | 2.454 |
| $CH_4$-$CO_2$ | −905.524 | 225 ($CO_2$) | 5.260 |

model from a microscopic perspective, the relative concentrations of different models after kinetic optimization were analyzed. Under different temperatures, the relative concentration distribution of $CH_4$, $CO_2$, and $N_2$ in the coal model along the z-axis is shown in Fig. 4. The data in the figure was the average relative concentration of the gases in the vacuum layer at different temperatures.

As shown in Fig. 4, the relative concentration of $CH_4$ in the vacuum layer increased upon the injection of $CO_2$ and $N_2$ in the model. As the temperature increased, the relative concentration of $CO_2$, $N_2$, and $CH_4$ in the vacuum layer increased, and the overall relationship was $CH_4$>$CO_2$>$N_2$. This change indicates that part of the $CH_4$ diffused into the slit area, and the relative concentration distribution of $CO_2$ and $N_2$ was still concentrated in the coal molecular layer. From a microscopic point of view, $CO_2$ and $N_2$ mainly drove off $CH_4$ by occupying adsorption sites. In the model, the effects of $CO_2$ and $N_2$ injection on the relative concentration of $CH_4$ differed. The average relative concentration of $CH_4$ in the $CH_4$-$N_2$ model increased from 0.180 to 0.245, and that in the $CH_4$-$CO_2$ model increased from 0.413 to 0.427. The relative concentration of $CH_4$ in the vacuum layer in the $CO_2$ injection model was high.

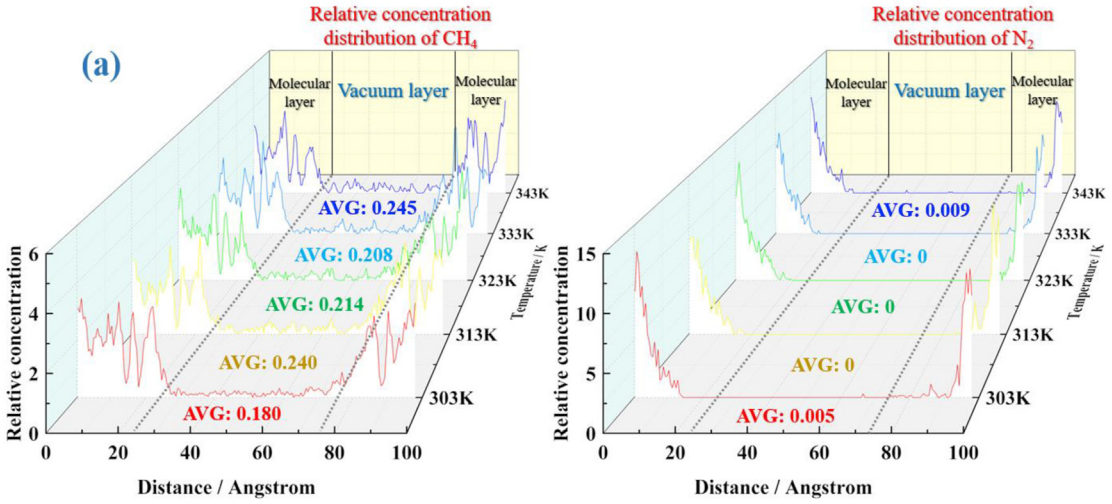


(a) The relative concentration distribution of $CH_4$ and $N_2$ in the coal model along the z–axis at different temperatures.

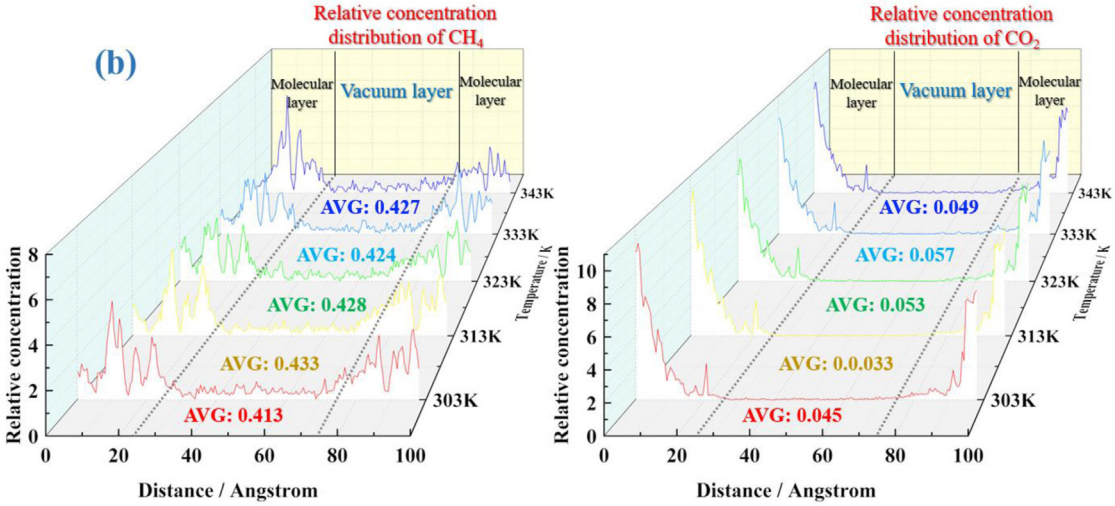


(b) The relative concentration distribution of $CH_4$ and $CO_2$ in the coal model along the z–axis at different temperatures.

**Fig. 4.** The relative concentration distribution of $CH_4$, $CO_2$, and $N_2$ in the coal model along the z-axis at different temperatures.

Comparing the average relative concentration of $CH_4$ in the $CH_4$-$N_2$ and $CH_4$-$CO_2$ models, it can be seen that the average relative concentration of $CH_4$ in the $CH_4$-$CO_2$ model is 1-2 times higher than that in the $CH_4$-$N_2$ model. Therefore, the effect of $CO_2$ injection was better than that of $N_2$ injection. The above simulation results are consistent with the experimental results of Wang L and Jessen K in enhanced coal bed methane recovery displacement experiments [9,42], which proves the reliability of the simulation results in this paper. In addition, Fig. 4 reflects the obvious symmetrical distribution of relative concentration. The region of 0-25 Å and 75-100 Å is the molecular layer of coal, and the region of 25-75 Å is the vacuum layer.

### 3.2. Diffusion laws of $CH_4$,$CO_2$,$N_2$ in coal model containing absorbed methane at different temperatures

#### 3.2.1. Mean square displacement curves of $CH_4$, $CO_2$, and $N_2$ at different temperatures

The model was dynamically optimized with the Focus module, and the NVT system was used in the optimization process. By analyzing the simulation results, the mean square displacement (MSD) curves of different models under varying temperatures were obtained. The formula for the MSD is as follows [43].

$$MSD = |r_i(t) - r_i(0)|^2 = \frac{1}{NN_t}\sum_{i=1}^{N}\sum_{t_0}^{N_t}|r_i(t+t_0) - r_i(t_0)|^2 = \lim_{t\to\infty}\frac{1}{N_t}\sum_{i=1}^{N}[r_i(t) - r_i(0)]^2 \quad (4)$$

In the formula, $N$ is the number of adsorbate molecules, $Nt$ is the statistical average number of molecular dynamics steps, $t$ is the simulation time (ps), and $r_i(t)$ and $r_i(0)$ are the position vectors of the $i$th particle at time $t$ and initial time, respectively. The setting parameters of the Focite module were as follows. The task item was Dynamics, the temperature was set at 303-343 K, the temperature control method was Nose, the pressure was 0.0001 GPa, the pressure control method was Berendsen, the number of steps was 10,000, the time step length was 1 fs, and the simulation time was 40 ps. At different temperatures, the MSD curves and desorption configurations of different models are shown in Fig. 5.

In Fig. 5, the MSD of all gases in the $CH_4$-$N_2$ and $CH_4$-$CO_2$ models showed a gradual increase with increasing temperature. The MSD represents the distance between the particle and the initial position at time $t$. The MSD of the gas increased with temperature, indicating that the molecular activity in the system increased with increasing temperature.

A comparison of the adsorption positions of $CO_2$ and $N_2$ in Fig. 5a and b revealed that that the two gases mainly drove $CH_4$ by occupying adsorption sites. The model injected with $CO_2$ had significantly more free methane molecules than the model with $N_2$, indicating that the effect of $CO_2$ injection on methane desorption was better than that of $N_2$. The change value of surface free energy of coal after $CO_2$ adsorption was generally larger than that after $CH_4$ adsorption. In addition, $CO_2$ exhibited multilayer adsorption on the surface of the coal matrix, while $CH_4$ and $N_2$ demonstrated monolayer adsorption. For a coal molecular structure with a fixed pore size distribution, the molecular dynamic diameter of the adsorbate ($CH_4$ is 0.38 nm, $N_2$ is 0.364 nm, and $CO_2$ is 0.33 nm) determined the effective pore segment that could enter the coal molecule. The pore diameter larger than the diameter of gas molecules in coal was the effective adsorption pore diameter. The relationship of molecular diameter in multi-component gas was $CH_4$>$N_2$>$CO_2$. The molecular diameter was inversely proportional to the adsorption capacity, which also confirmed that the adsorption performance of $CO_2$ was better than that of $CH_4$ and $N_2$.

Under different temperatures, the mean square displacement of $CH_4$ in the $CH_4$-$CO_2$ model was greater than that in the $CH_4$-$N_2$ model, with growth rates of 35.22% (303K), 25.33% (313K), 34.41% (323K), 31.39% (333K) and 0.57% (343K). This indicated that the molecular activity in the $CH_4$-$CO_2$ model was higher, so the $CO_2$ had a better effect of promoting methane desorption. It is consistent with the experimental results of Tu Y [44] , Wu D [45], and Yu H [46] in the laboratory, which confirms the reliability of the simulation in this paper.

#### 3.2.2. Diffusion coefficients of $CH_4$, $CO_2$, and $N_2$ at different temperatures

The diffusion coefficient was calculated using the MSD curve and the Einstein method, where the Einstein formula is expressed as follows [43].

$$D = \frac{1}{6N}\lim\frac{d}{dt}\left\langle\sum_{i=1}^{N}[r_i(t) - r_i(0)]\right\rangle^2 \quad (5)$$

In the formula, $D$ is the diffusion coefficient ($m^2/s$), $N$ is the number of adsorbate molecules, $t$ is the simulation time ($ps$), and $r_i(t)$ and $r_i(0)$ are the position vectors of the $i$th particle at time $t$ and initial time, respectively. Linear regression was performed on the MSD curves to obtain the slope $k$, and the diffusion coefficient $D$ could be simplified to the following formula [43].

$$k = \lim_{t\to\infty}\frac{1}{t}\left\langle\frac{1}{N_t}\sum_{i=1}^{N}\left|r_i(t) - r_i(0)\right|^2\right\rangle \quad (6)$$

$$D = \frac{k}{6} \quad (7)$$

Fig. 6 shows the fitting curves of diffusion coefficients of different gases at varying temperatures. Fig. 7 shows the relationship between the diffusion coefficients of different gases and the temperature.

Fig. 6 shows that the MSD of the gases in the $CH_4$-$N_2$ and $CH_4$-$CO_2$ models both increased with time; under the same time, the MSD of the gases increased with increasing temperature. As shown in Fig. 6, the fitting degrees $R^2$ of the curves were all greater than 0.98, which was relatively high, thereby ensuring the reliability of the calculated diffusion coefficient $D$. As the temperature increased, the diffusion coefficient of the gas gradually increased. The higher the temperature, the greater the molecular internal energy. According to the principle of energy conservation, internal energy will be converted into kinetic energy to make the molecules move violently. Therefore, the higher the temperature, the greater the diffusion rates of the gas, the easier it is to diffuse out of the coal seam [47].

Fig. 7 shows that the influence of the injection of $N_2$ and $CO_2$ on the diffusion coefficient of $CH_4$ increased with temperature. The diffusion coefficients of $CH_4$, $N_2$, and $CO_2$ reported in the literature are within the ranges of $10^{-11}$-$10^{-9}$ $m^2/s$ [48,49], $10^{-10}$-$10^{-9}$ $m^2/s$ [50], and $10^{-10}$-$10^{-9}$ $m^2/s$ [51], respectively. Furthermore, the diffusion coefficients of $CH_4$($CH_4$-$N_2$ model), $CH_4$($CH_4$-$CO_2$ model), $N_2$, and $CO_2$ at 303K-343K in this study were calculated to be $7.902\times10^{-10}$ - $2.379\times10^{-9}$ $m^2/s$, $1.094\times10^{-9}$ - $2.367\times10^{-9}$ $m^2/s$, $1.562\times10^{-10}$ - $2.405\times10^{-10}$ $m^2/s$, and $1.337\times10^{-10}$ - $1.837\times10^{-10}$ $m^2/s$, respectively, which are in close agreement with the reference values. There was a linear positive correlation between temperature and diffusion coefficient, and the relationship between the diffusion coefficients of the three gases is $CO_2$ < $N_2$ <

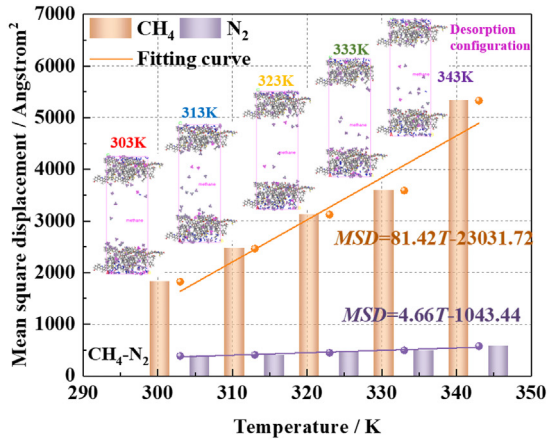


(a) The MSD curves and desorption configurations of $CH_4$–$N_2$ model at different temperatures.

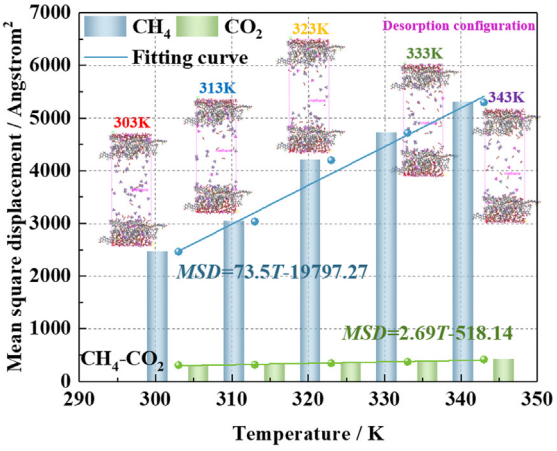


(b) The MSD curves and desorption configurations of $CH_4$–$CO_2$ model at different temperatures.

**Fig. 5.** The MSD curves and desorption configurations of different models at different temperatures.

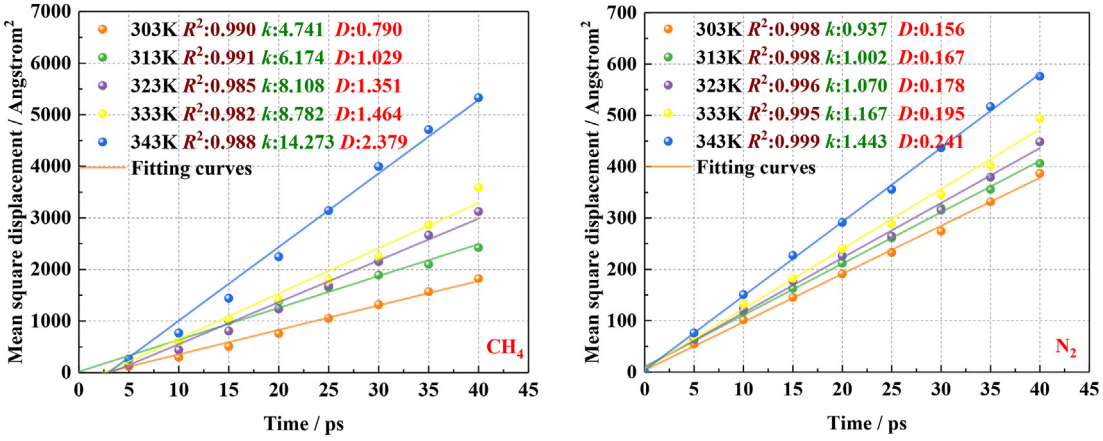


(a) The fitting curves of diffusion coefficients of $CH_4$ and $N_2$ in the coal model at different temperatures.

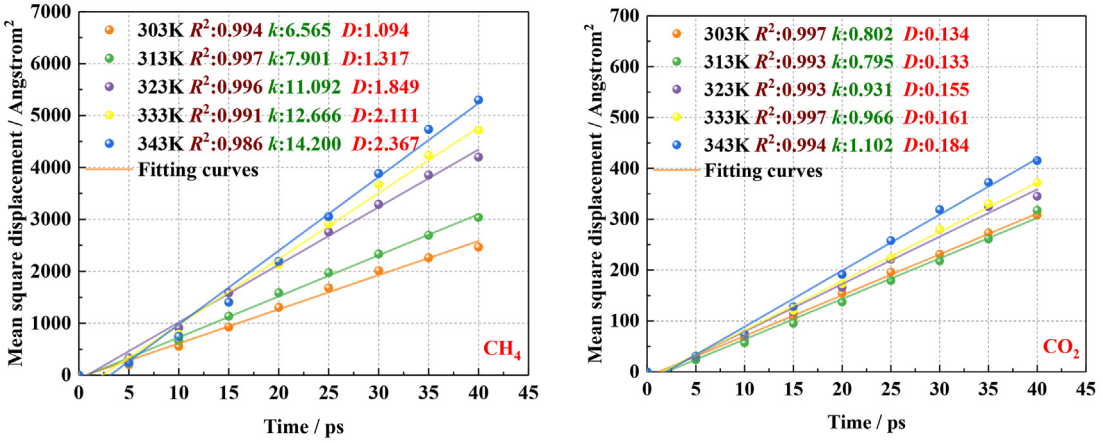


(b) The fitting curves of diffusion coefficients of $CH_4$ and $CO_2$ in the coal model at different temperatures.

**Fig. 6.** The fitting curves of diffusion coefficients of $CH_4$, $CO_2$, and $N_2$ in the coal model at different temperatures.

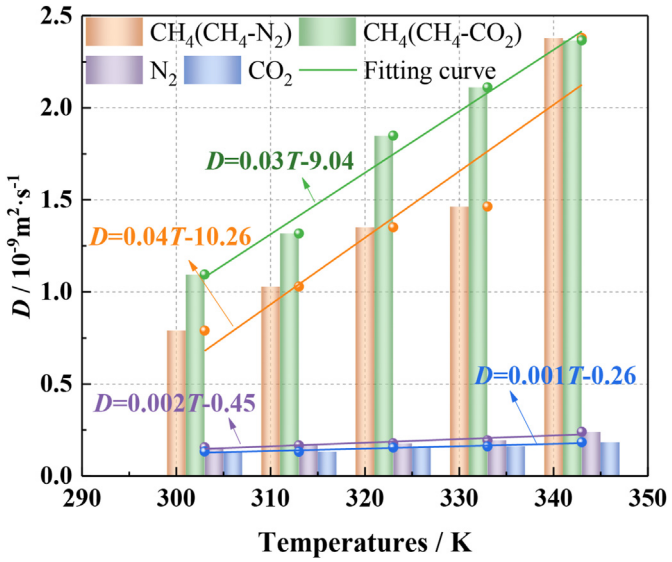


**Fig. 7.** The relationship between the diffusion coefficients of different gases and the temperature.

Diffusion activation energy represents the energy required for 1 mol atom to perform diffusion motion. As shown in Fig. 8, in the $CH_4$-$N_2$ and $CH_4$-$CO_2$ models, the relationship of the diffusion activation energy of the three gases was $CH_4$>$N_2$>$CO_2$. In general, as the experimental temperature increases, the diffusion phenomenon becomes more significant, the diffusion activation energy decreases, the diffusion coefficient of the molecule increases, and diffusion occurs easily. By contrast, as the temperature increases, the gas molecules gain energy, turning a portion of the molecules with low original energy into activated molecules and increasing the percentage of activated molecules, which increases the number of effective collisions and the diffusion rate. When the temperature rises, the molecular motion speeds up and the reaction speeds up as the number of collisions of reactants per unit time increases. Diffusion activation energy reflects the sensitivity of diffusion motion to temperature. The diffusion activation energy of $CH_4$ in the $CH_4$-$N_2$ and $CH_4$-$CO_2$ models was 5.26 and 4.18 kcal/mol, respectively. In the model of $CO_2$ injection, the diffusion activation energy of $CH_4$ was reduced by 20.53%, indicating that the displacement effect of $CO_2$ injection was better than that of $N_2$ injection.

To further research the effects of $CO_2$ and $N_2$ on promoting the

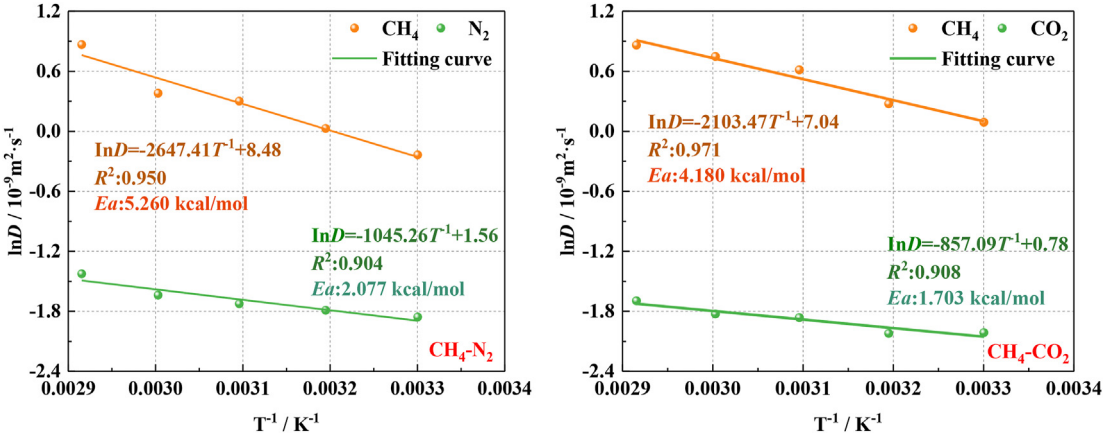


**Fig. 8.** The fitting curves of the relationship between ln$D$ and $T^{-1}$ of different models.

$CH_4$. In the $CH_4$-$N_2$ model, the diffusion coefficient of $CH_4$ in the vacuum layer increased with temperature, and the growth rates were 20.35% (313K), 40.39% (323K), 14.19% (333K), 12.11% (343K). In the $CH_4$-$CO_2$ model, the diffusion coefficient of $CH_4$ in the vacuum layer increased with temperature, and the growth rates were 30.23% (313K), 31.32% (323K), 8.31% (333K), 62.53% (343K).

### 3.3. Diffusion activation energy and velocity distribution of $CH_4$, $CO_2$, and $N_2$ at different temperatures

To research the influence of different temperatures on gas diffusion, we calculated the diffusion activation energy of gases through the Arrhenius equation. The formula is as follows [43].

$$D = D_0 exp\left(-\frac{E_a}{RT}\right) \quad (8)$$

In the formula, $D_0$ is the pre-exponential factor ($m^2/s$), $E_a$ is the apparent activation energy (kcal/mol), and $R$ is the perfect gas constant (kcal/(mol·K)). The curve of the relationship between the diffusion coefficient and the reciprocal of temperature was fitted. The diffusion activation energy was calculated, as shown in Fig. 8.

desorption of $CH_4$ from a microscopic perspective, velocity analysis was performed on different models after kinetic optimization. Under different temperatures, the velocity distribution of $CH_4$, $CO_2$, and $N_2$ in the coal model along the z-axis is shown in Fig. 9. The signs of velocity represents the direction of motion, so here is the average of absolute values of velocity.

As shown in Fig. 9, the molecular motion velocity of $CH_4$ in the vacuum layer increased after the injection of $CO_2$ and $N_2$ in the models. This result suggested that some of $CH_4$ diffused into the vacuum layer. The velocity distribution of $N_2$ was mainly concentrated in the coal molecular layer, while the velocity distribution of $CO_2$ was distributed in the whole region. With the increased of temperature, the motion velocity of $CH_4$ in the vacuum layer increased. The relationship of the average velocity distribution of the three gases in the vacuum layer was $CH_4$>$CO_2$>$N_2$. Comparing the average velocity of $CH_4$ in the vacuum layer in different models, under different temperature conditions, the average velocity of $CH_4$ in the $CH_4$-$CO_2$ model were 34.26% (303K), 27.27% (313K), 10.11% (323K), 39.72% (333K), and 24.16%(343K) lower than that in the $CH_4$-$N_2$ model. Combined with the results of the relative concentration distribution in Fig. 4, although $CO_2$ showed a significant

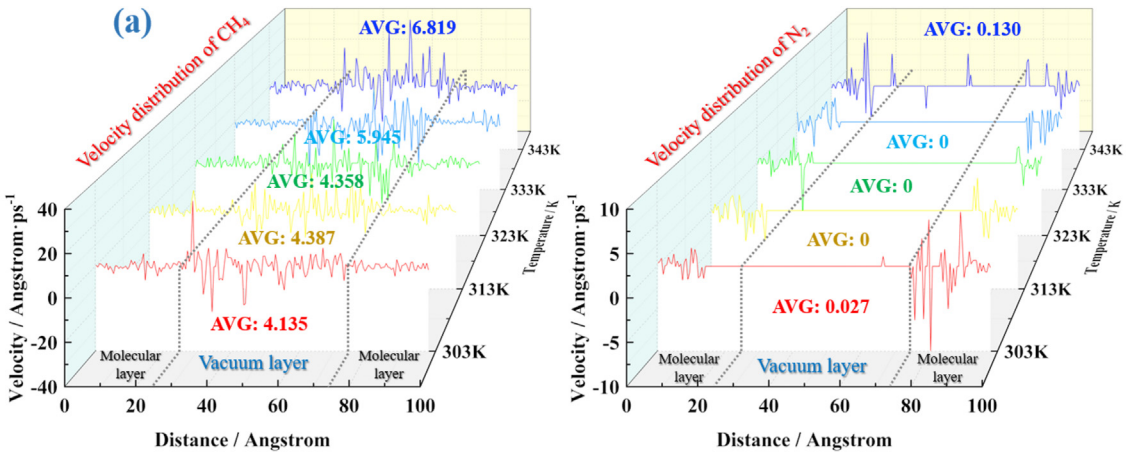


(a) The velocity distribution of $CH_4$ and $N_2$ in the coal model along the z–axis at different temperatures.

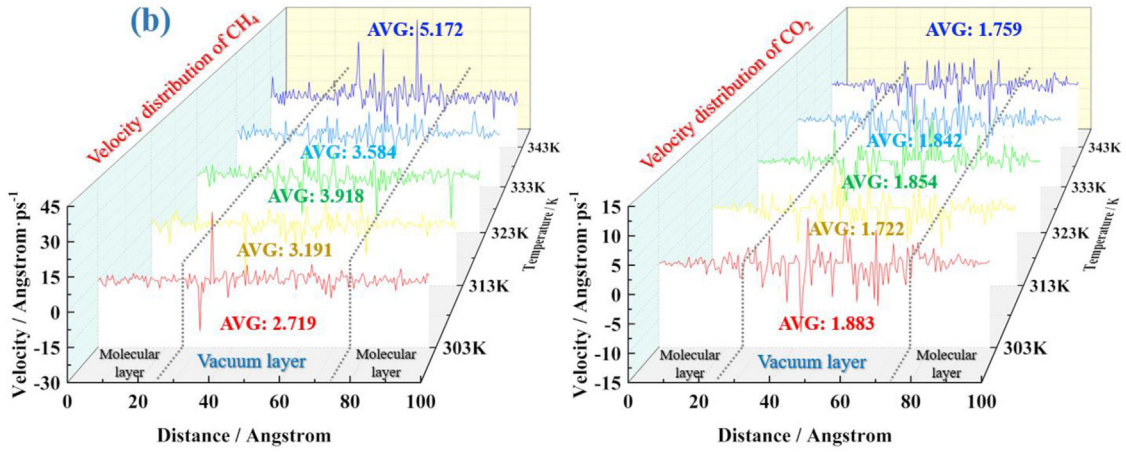


(b) The velocity distribution of $CH_4$ and $CO_2$ in the coal model along the z–axis at different temperatures.

**Fig. 9.** The velocity distribution of $CH_4$, $CO_2$, and $N_2$ in the coal model along the z-axis at different temperatures.

velocity distribution in the vacuum layer, the concentration was very low, so the velocity distribution was consistent with the diffusion law obtained in 3.2.

## 4. Conclusions

- $CO_2$ and $N_2$ mainly drive $CH_4$ by occupying adsorption sites. The model injected with $CO_2$ exhibited significantly more free methane molecules than that with $N_2$. The total energy of the initial model and desorption model of the $CH_4$-$N_2$ and $CH_4$-$CO_2$ systems both increased with the increase of temperature. The $CH_4$-$CO_2$ model was more stable than the $CH_4$-$N_2$ model from a microscopic perspective.
- With the increased of temperature, the average relative concentration and motion velocity of $CH_4$ in the vacuum layer increased. The relationship of the average relative concentration and average velocity distribution of the three gases in the vacuum layer was $CH_4$>$CO_2$>$N_2$.
- Under the same time conditions, the relationship between the mean square displacement and diffusion coefficient of $CH_4$, $CO_2$, and $N_2$ in different models was $CH_4$>$CO_2$>$N_2$, and they all increased with temperature.
- The relationship of the diffusion activation energy of the three gases was $CH_4$>$N_2$>$CO_2$. The diffusion activation energy of $CH_4$ in $CH_4$-$N_2$ and $CH_4$-$CO_2$ models was 5.26 and 4.18 kcal/mol, respectively. In the model of $CO_2$ injection, the diffusion activation energy of $CH_4$ was reduced by 20.53%.

- The effect of $CO_2$ injection on methane desorption was better than that of $N_2$. This paper can provide some basis for the research and development of gas injection technology in coal seam.
- This research can provide a theoretical basis for the development of coal seam gas injection stimulation technology. Subsequent research will combine specific coal and rock parameters to refine the research results.

## Credit author statement

The paper was completed by the listed authors. Yang Bai: Conceptualization, Formal analysis, Data curation, Writing - original draft. Hai-fei Lin*: Writing - review & editing, Methodology, Funding acquisition. Shu-Gang Li: Validation, Funding acquisition. Min Yan: Methodology. Hang Long: Appropriate words.

## Declaration of competing interest

The authors declare that they have no known competing financial interests or personal relationships that could have appeared to influence the work reported in this paper.

## Acknowledgements

This research was supported financially by the National Natural Science Foundation of China (5173-4007, 5167-4192, 5187-4236), National Natural Science Foundation of Shaanxi Province (2020JC-48, 2019JLP-02). The use of the Materials Studio software package, which was supported by the College of Chemistry and Chemical Engineering of Xi'an University of Science and Technology, is gratefully acknowledged.

## Appendix A. Supplementary data

Supplementary data to this article can be found online at https://doi.org/10.1016/j.energy.2020.119686.

## References

[1] Ying LM, Chen J, Du C, Pang LX, Wen YJ. The research progress of coal and gas co-mining. Adv Mater Res 2012;524-527:489–93.
[2] Karacan CÖ, Ruiz FA, Cotè M, Phipps S. Coal mine methane: a review of capture and utilization practices with benefits to mining safety and to greenhouse gas reduction. Int J Coal Geol 2011;86:121–56.
[3] Xie KC. The structure and reactivity of coal. Beijing: Science Press; 2002. p. 46–50.
[4] Chen ZL, Xu WR, Tang LD. The theory and Practice of molecular simulation. Beijing: Chemical Industry Press; 2007. p. 79–80.
[5] Irfan MF, Usman MR, Kusakabe K. Coal gasification in $CO_2$, atmosphere and its kinetics since 1948: a brief review. Energy 2011;36(1):12–40.
[6] Kumar H, Elsworth D, Mathews JP. Effect of $CO_2$ injection on heterogeneously permeable coalbed reservoirs. Fuel 2014;135:509–21.
[7] Wang QQ, Li W, Zhang DF, Wang HH, Jiang WP, Li Z, et al. Influence of high-pressure $CO_2$, exposure on adsorption kinetics of methane and $CO_2$ on coals. J Nat Gas Sci Eng 2016;34:811–22.
[8] Bhowmik S, Dutta P. Investigation into the methane displacement behavior by cyclic, pure carbon dioxide injection in dry, powdered, bituminous Indian coals. Energy Fuel 2011;25(6):2730–40.
[9] Jessen K, Tang GQ, Kovscek AR. Laboratory and simulation investigation of enhanced coalbed methane recovery by gas injection. Transport Porous Media 2008;73:141–59.
[10] Han F, Busch A, Krooss BM. $CH_4$ and $CO_2$ sorption isotherms and kinetics for different size fractions of two coals. Fuel 2013;108(6):137–42.
[11] Fan YP, Deng CB, Xun Z, Li FQ, Wang XY, Qiao L, et al. Numerical study of $CO_2$-enhanced coalbed methane recovery. Int J Greenh Gas Con 2018;76(9):12–23.
[12] Huo PL, Zhang DF, Yang Z. $CO_2$ geological sequestration: displacement behavior of shale gas methane by carbon dioxide injection. Int J Greenh Gas Con 2017;66:48–59.
[13] Kong LD, Zou RY, Bi WZ, Zhong RQ, Mu WJ, Liu J, et al. Selective adsorption of $CO_2/CH_4$ and $CO_2/N_2$ within a charged metal-organic framework. J Mater Chem 2014;2:139–42.
[14] Topolnicki J, Kudasik M, Dutka B. Simplified model of the $CO_2/CH_4$ exchange sorption process. Fuel Process Technol 2013;113:67–74.
[15] Eshkalak MO, Alshalabi EW, Sanaei A. Simulation study on the $CO_2$-driven enhanced gas recovery with sequestration versus the refracturing treatment of horizontal wells in the U.S. unconventional shale reservoirs. J Nat Gas Sci Eng 2014;21:1015–24.
[16] Crosdale PJ, Moore TA, Mares TE. Influence of moisture content and temperature on methane adsorption isotherm analysis for coals from a low-rank, biogenically-sourced gas reservoir. Int J Coal Geol 2008;76:166–74.
[17] Wang Z, Tang X, Yue G, Kang B, Xie C, Li X. Physical simulation of temperature influence on methane sorption and kinetics in coal: benefits of temperature under 273.15K. Fuel 2015;158:207–16.
[18] Charoensuppanimit P, Mohammad SA, Robinson RL, Gasem KA. Modeling the temperature dependence of supercritical gas adsorption on activated carbons, coals and shales. Int J Coal Geol 2015;138:113–26.
[19] Guan C, Liu S, Li C, Wang Y, Zhao Y. The temperature effect on the methane and $CO_2$ adsorption capacities of Illinois coal. Fuel 2018;211:241–50.
[20] Li SG, Bai Y, Lin HF, Shu CM, Yan M, Laiwang B. Molecular simulation of adsorption of gas in coal slit model under the action of liquid nitrogen. Fuel 2019;255:115775.
[21] Meng ZY, Yang ZY, Yin ZQ, Li YY, Ju XQ, Yao YQ, et al. Interaction between dispersant and coal slime added in semi-coke water slurry: an experimental and DFT study. Appl Surf Sci 2020;540:148327.
[22] Matranga KR, Myers AL, Glandt ED. Storage of natural gas by adsorption on activated carbon. Chem Eng Sci 1992;47:1569–79.
[23] Liu XQ, He X, Qiu NX, Yang X, Tian ZY, Li MJ. Molecular simulation of $CH_4$, $CO_2$, $H_2O$ and $N_2$ molecules adsorption on heterogeneous surface models of coal. Appl Surf Sci 2016;389:894–905.
[24] Mosher K, He JJ, Liu YY, Rupp E, Wilcox J. Molecular simulation of methane adsorption in micro- and mesoporous carbons with applications to coal and gas shale systems. Int J Coal Geol 2013;109:36–44.
[25] Hu HX, Du L, Xing YF, Li XC. Detailed study on self- and multicomponent diffusion of $CO_2$–$CH_4$, gas mixture in coal by molecular simulation. Fuel 2017;187:220–8.
[26] You J, Tian L, Zhang C, Yao HX, Dou W, Fan B, et al. Adsorption behavior of carbon dioxide and methane in bituminous coal: a molecular simulation study. Chin J Chem Eng 2016;24:1275–82.
[27] Sun X, Zhang Y, Li K, et al. A new mathematical simulation model for gas injection enhanced coalbed methane recovery. Fuel 2016;183(12):478–88.
[28] Liu Y, Zhu YM, Liu SM, Li W, Tang X. Temperature effect on gas adsorption capacity in different sized pores of coal: experiment and numerical modeling. J Petrol Sci Eng 2018;165:821–30.
[29] Ju Y, He J, Chang E, Chang ES, Zheng LG. Quantification of $CH_4$ adsorption capacity in kerogen-rich reservoir shales: an experimental investigation and molecular dynamic simulation. Energy 2018;170:411–22.
[30] Tao HH, Zhang LH, Liu QG, Zhao YL, Feng Q. Competitive adsorption and selective diffusion of $CH_4$ and the intruding gases in coal vitrinite. Energy Fuel 2019;33(8):6971–82.
[31] Liu XQ, Li MJ, Zhang CH, Fang RH, Zhong NN, Xue Y, et al. Mechanistic insight into the optimal recovery efficiency of CBM in sub-bituminous coal through molecular simulation. Fuel 2020;266:117137.
[32] Wiser WH, Hill GR, Kertamus NJ. Kinetic study of pyrolysis of high volatile bituminous coal. Ind Eng Chem Process Des Dev 1967;2(1):133–8.
[33] Carlson GA. Computer simulation of the molecular structure of bituminous coal. Energy Fuel 1992;6(6):771–8.
[34] Sun H, Ren P, Fried JR. The COMPASS force field: parameterization and validation for phosphazenes. Comput Theor Polym Sci 1998;8:229–46.
[35] Sun HJ. COMPASS: an ab initio force-field optimized for condensed-phase Applications overview with details on alkane and benzene compounds. J Phys Chem B 1998;102:7338–64.
[36] Yin T, Liu D, Cai Y, Liu ZH. A new constructed macromolecule-pore structure of anthracite and its related gas adsorption: a molecular simulation study. Int J Coal Geol 2020;220:103415.
[37] Hu H, Li X, Fang Z, Wei N, Li QS. Small-molecule gas sorption and diffusion in coal: molecular simulation. Energy 2010;35(7):2939–44.
[38] Kawai S, Foster AS, Björkman T. Van der Waals interactions and the limits of isolated atom models at interfaces. Nat Commun 2016;7:11559.
[39] Delville A, Pellenq RJM. Electrostatic attraction and/or repulsion between charged colloids: a (NVT) monte-carlo study. Mol Simulat 2000;24(1-3):1–24.
[40] Fifield LS, Grate JW. Hydrogen-bond acidic functionalized carbon nanotubes (CNTs) with covalently-bound hexafluoro isopropanol groups. Carbon 2010;48(7):2085–8.
[41] Meng ZP, Tian YD, Li GF. Theories and methods of coalbed methane development geology. Beijing: Science Press; 2010.
[42] Wang L, Wang Z, Li K, Chen HD. Comparison of enhanced coalbed methane recovery by pure $N_2$ and $CO_2$ injection: experimental observations and numerical simulation. J Nat Gas Sci Eng 2015;23:363–72.
[43] Yang JZ, Liu QL, Wang HT. Analyzing adsorption and diffusion behaviors of ethanol/water through silicalite membranes by molecular simulation. J membrane sci 2007;291(1-2):1–9.
[44] Tu Y, Xie CL, Li RM. The contrast experimental study of displacing coalbed methane by injecting carbon dioxide or nitrogen. Adv Mater Res 2013;616-618:778–85.
[45] Wu D, Liu X, Liang B, Sun KM, Xiao XC. Experiments on displacing methane in

coal by injecting supercritical carbon dioxide. Energy Fuel 2018;32(12):12766–71.
[46] Yu H, Yuan J, Guo W, Chen JL, Hu QT. A preliminary laboratory experiment on coalbed methane displacement with carbon dioxide injection. Int J Coal Geol 2008;73(2):156–66.
[47] Kelemen SR, Kwiatek LM. Physical properties of selected block Argonne Premium bituminous coal related to $CO_2$, $CH_4$, and $N_2$ adsorption. Int J Coal Geol 2009;77(1-2):2–9.
[48] Xu H, Tang DZ, Zhao JL, Li S, Tao S. A new laboratory method for accurate measurement of the methane diffusion coefficient and its influencing factors in the coal matrix. Fuel 2015;158:239–47.
[49] Gao D, Hong L, Wang J. Molecular simulation of gas adsorption characteristics and diffusion in micropores of lignite. Fuel 2020;269:117443.
[50] Zhao W, Cheng YP, Jiang HN, Wang HF, Li W. Modeling and experiments for transient diffusion coefficients in the desorption of methane through coal powders. Int J Heat Mass Tran 2017;110:845–54.
[51] Saghafi A, Faiz M, Roberts D. $CO_2$ storage and gas diffusivity properties of coals from Sydney Basin, Australia. Int J Coal Geol 2007;70(1-3):240–54.